



Spectroelectrochemical properties of ultra-thin indium tin oxide films under electric potential modulation



Xue Han ^{*,1}, Sergio B. Mendes ²

Department of Physics and Astronomy, University of Louisville, Louisville, KY 40208, United States

ARTICLE INFO

Article history:

Received 22 May 2015

Received in revised form 7 February 2016

Accepted 9 February 2016

Available online 11 February 2016

Keywords:

Indium tin oxide

Spectroelectrochemistry

Cyclic voltammetry

AC impedance potential modulation

Integrated optical waveguide

Absorbance spectroscopy

ABSTRACT

In this work, the spectroscopic properties of ultra-thin ITO films are characterized under an applied electric potential modulation. To detect minute spectroscopic features, the ultra-thin ITO film was coated over an extremely sensitive single-mode integrated optical waveguide, which provided a long pathlength with more than adequate sensitivity for optical interrogation of the ultra-thin film. Experimental configurations with broadband light and several laser lines at different modulation schemes of an applied electric potential were utilized to elucidate the nature of intrinsic changes. The imaginary component of the refractive index (absorption coefficient) of the ultra-thin ITO film is unequivocally shown to have a dependence on the applied potential and the profile of this dependence changes substantially even for wavelengths inside a small spectral window (500–600 nm). The characterization technique and the data reported here can be crucial to several applications of the ITO material as a transparent conductive electrode, as for example in spectroelectrochemical investigations of surface-confined redox species.

Published by Elsevier B.V.

1. Introduction

Because of its good optical transparency and electrical conductivity, films of indium tin oxide (ITO) have been widely used in solar cells [1–3], displays [4,5], electrochromic devices [6,7], LEDs [8–10], and spectroelectrochemical applications [11,12]. ITO films in the thickness range of about 100 nm to 1 μm that had been grown by different deposition techniques and treated under diverse annealing conditions have been extensively investigated [13–16]. The conductivity and transparency of these films, and their relationship to the film crystalline structure have been widely studied [13]. However, those studies have been implemented for relatively thick ITO films (above 100 nm) because it becomes particularly challenging to characterize the spectroscopic features of thinner (e.g., below 30 nm) ITO films. The optical transparency and spectroscopic features of very thin ITO films cannot be precisely addressed by conventional transmission measurements and advanced characterization techniques are required in these cases. Another important limitation has been the lack of information on how the spectroscopic properties of the ITO film behave under potential modulations, which is crucial to understand the performance of those films at working conditions in a variety of applications. Only a few studies have been reported on the electrical properties of ITO films under potential modulations

in different solution and electrolyte conditions [17–20], and on the refractive index of ITO films under potential modulation [21,22], however those studies were limited to relatively thick ITO films.

In this present work, we apply an integrated optical waveguide technique to study the spectroscopic optical characteristics of ultra-thin ITO films. A planar, single-mode, integrated optical waveguide (IOW) creates a highly sensitive platform to investigate the spectroscopic properties of an overcoated ultra-thin ITO film. We report here investigations on the spectroscopic properties of ultra-thin ITO films performed under aqueous environment and different electric potential modulation approaches, which represent the working conditions present in many of the applications of ITO films. It is expected that the electrical modulation and environmental conditions will have a stronger impact in the properties of thinner films, as opposed to the thicker ones, and we aimed to address those effects in this work. Understanding the spectroscopic features of ultra-thin ITO films under those conditions is particularly critical for spectroelectrochemical and electro-optical applications that utilize an ITO film as a transparent working electrode [23].

2. Thick ITO films

2.1. Sample preparation

The ITO fabrication process was first optimized to create films with extremely low optical attenuation and good electrical conductivity. For this purpose, relatively thicker ITO films (ca. 400 nm) were deposited on plain glass slides to identify the best fabrication conditions. Once those conditions were established, such protocol was then applied to

* Corresponding author at: Department of Physics and Astronomy, University of Louisville, KY, 40208, USA.

E-mail addresses: x0han004@louisville.edu (X. Han), sbmend01@louisville.edu (S.B. Mendes).

¹ Tel.: +1 502 510 3917.

² Tel.: +1 502 852 0908; fax: +1 502 852 0742.

deposit ultra-thin ITO films (ca. 13 nm) over single-mode IOW devices described in Section 3.

A pulsed-DC sputtering technique was used to deposit ITO films from a 3-inch target of $(\text{In}_2\text{O}_3)_{90}:(\text{SnO})_{10}$ wt.% and 99.99% purity. The power of the pulsed-DC sputtering was set at 200 W with a frequency of 20 kHz and a pulse duration of 1 μs . The substrates were kept at room temperature during deposition and the rotation speed of the substrate table was set at 20 rpm to achieve uniform films. The flow rate of Ar was fixed at 12 sccm and different flow rates of O_2 were explored (0.4 sccm to 0.8 sccm) to optimize the electrical and optical properties of the ITO film. For each O_2 flow rate, a 30-min deposition process was used to grow a film with a thickness of approximately 400 nm. After the deposition process, an inert annealing treatment in N_2 atmosphere at 250 °C for 10 min was used to activate Sn element, create additional oxygen vacancies, and minimize grain boundary effects to obtain lower resistivity and better transparency in the visible range [24].

2.2. Optical and electrical properties

Transmittance spectra of the thicker ITO samples were measured by a conventional spectrophotometer (Cary 300, Varian). An envelope technique [25] based on the transmittance spectra was employed to determine the thickness and refractive index (both real and imaginary parts) of the ITO films. The sheet resistance and thickness of the film were then used to calculate the film resistivity. In Fig. 1(a) and (b), the extinction coefficient (imaginary part of the refractive index) at the 550 nm wavelength and the resistivity are shown against the O_2 flow rate during the sputtering deposition process. And those properties are compared for samples as sputtered and after the inert annealing treatment.

For the optical performance of samples before the inert annealing process, we observe in Fig. 1 (a) that the extinction coefficient decreases as the O_2 flow rate increases from 0.40 to 0.65 sccm, and remains approximately constant above 0.65 sccm. The inert annealing process substantially reduces the extinction coefficient for samples deposited under low O_2 flow rate (i.e. high values of the extinction coefficients), while the minimum extinction coefficient was found with an O_2 flow rate of about 0.6 sccm. For the electrical resistivity (see Fig. 1b), we notice that regardless of the O_2 flow rate during deposition the inert annealing process consistently improves the electrical conductivity of the film probably by minimizing grain boundary defects in the films [26]. However, when the O_2 flow rate increases, the electrical performance of annealed samples shows a monotonic increase in their resistivity. A flow rate of 0.6 sccm for the O_2 gas during the sputtering process to deposit ultra-thin ITO films was established based on these measurements.

3. Ultra-thin ITO films

3.1. Sample preparation

Planar, single-mode, integrated optical waveguide platforms have been used in challenging studies of adsorbed molecular thin films [27–30] due to their long effective pathlength. The strong optical interaction of a guided mode with a surface-adsorbed molecular assembly has enabled highly sensitive studies of weakly absorbing structures. Fig. 2 schematically shows the IOW structure employed in this work to investigate the spectroscopic properties of ultra-thin films of the ITO material. Two surface-relief gratings (25.4 mm apart from each other) with a pitch size of 323 nm were initially fabricated on glass substrates (75 × 25 mm) to work as integrated waveguide couplers. A highly transparent, single-mode, planar IOW device was created on those glass slides by depositing a 400-nm layer of Al_2O_3 and a 16-nm layer of SiO_2 using an atomic layer deposition (ALD) process. Details of this fabrication process have been reported by us in the literature [30].

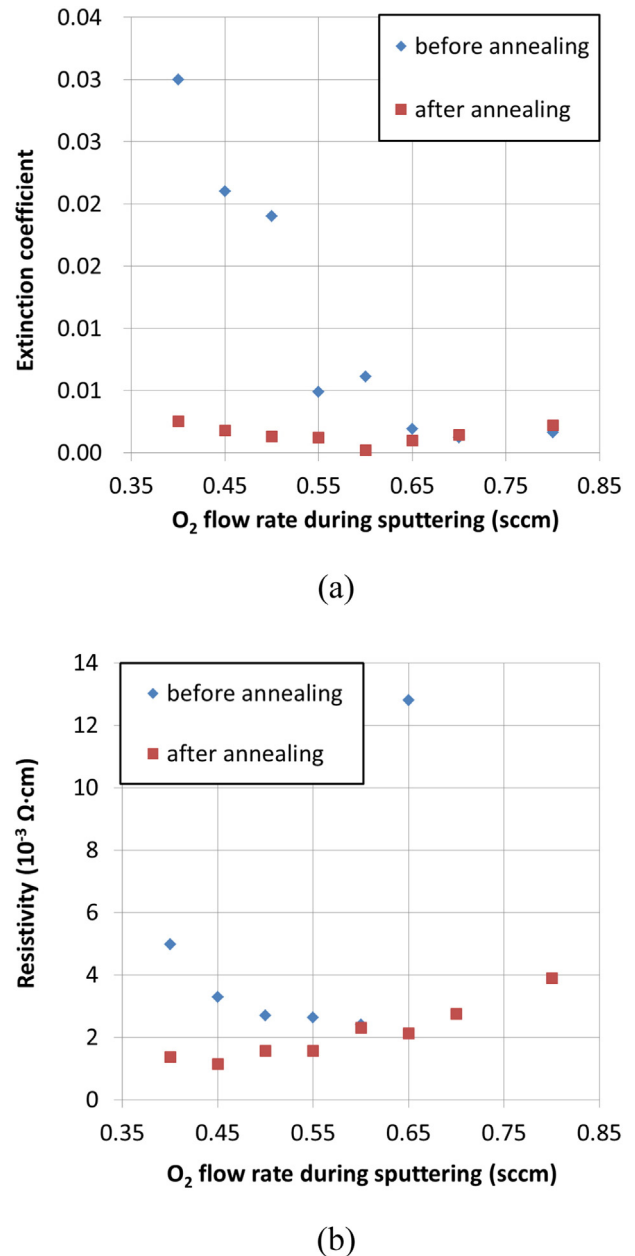


Fig. 1. Effects of O_2 flow rate during the sputtering deposition process on the optical and electrical properties of the ITO film with data provided for measurements before and after an inert annealing treatment. Experimental data of (a) the extinction coefficient (imaginary part of the refractive index) at 550 nm, and (b) the electrical resistivity. As the resistivity before the annealing process is very high at increased levels of O_2 flow rate, the measured resistivity data at 0.70 sccm (2.7 $\Omega\cdot\text{cm}$) and 0.80 sccm (not conductive) are not displayed in Fig. 1b.

Based on the experimental results described in Section 2 for the (relatively) thicker ITO films, a flow rate of 0.6 sccm for the O_2 gas was selected to deposit a 13-nm ITO film over single-mode IOW devices. After deposition, the same inert annealing process (previously described) was carried out for the ultra-thin ITO films, which provided films with consistently low resistivity values ($\rho = 2.3 \times 10^{-3} \Omega\cdot\text{cm}$). However, the extinction coefficient did not decline to the expected value ($k = 1.7 \times 10^{-4}$) and an annealing process in the presence of O_2 (called reactive annealing) was added to increase the optical transparency of the ultra-thin ITO films in the visible region. By annealing the samples in the presence of atmospheric oxygen, it is expected that oxygen vacancies in the film to decrease leading to a more complete stoichiometry in the ITO film. The fewer defects in the film should translate

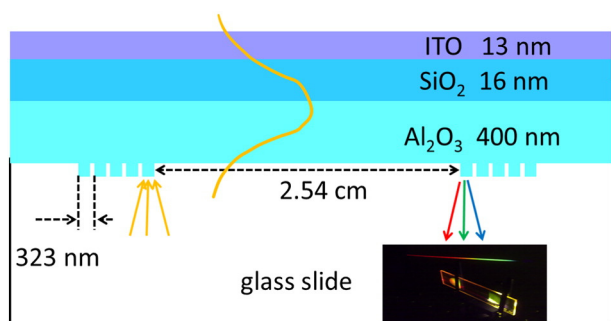


Fig. 2. Schematic structure of the single-mode integrated optical waveguide with an over-layer of an ultra-thin ITO film under investigation. An actual IOW device with broadband light dispersion of the out-coupled guided optical beam is shown in the inset.

into lower residual absorption, and thus lower propagation losses for the waveguide modes. We started the reactive annealing process at 150 °C and, when the optical performance was still insufficient, the temperature was raised by increments of 50 °C. A sample was heated until an acceptable optical loss for the IOW device overcoated with an ultra-thin ITO film was achieved. With this reactive annealing process, a total propagation loss of as low as 6 dB/cm was reached for the whole waveguide stack, which includes the Al₂O₃ and SiO₂ films and the ultra-thin ITO film. The sheet resistance was about 2 kΩ, which consistently corresponds to a value of $2.6 \times 10^{-3} \Omega \text{ cm}$ for the resistivity of the ITO film.

3.2. Spectroelectrochemical flowcell

Samples with low optical losses were placed in a buffer solution (Na₂PO₄, 5 mM, pH 7) for at least 24 h to chemically stabilize the ITO film. Then each sample was rinsed with DI water, dried by N₂ gas, and set for electrical connections. A piece of carbon tape was used to attach a platinum wire onto the ITO film for electrical connection to the potentiostat (CHI 600D). A layer of silver paste was placed around the two gratings to provide a uniform electric potential for the whole ITO film. After the silver paste became dry, an insulating epoxy layer was placed over it to prevent any chemical reaction between the silver paste and the working electrolyte solution. After the epoxy layer was cured, the insulation between the epoxy layer and the platinum wire was tested, as well as the conduction between the platinum wire and the ITO film, which serves as the working electrode in our experiments. A homemade pseudo-reference electrode of Ag/AgCl and a platinum counter electrode were inserted through the flow cell cover. The three electrodes were then connected to the potentiostat. The homemade pseudo-reference electrode in our electrolyte solution had a fairly constant potential offset of 85 mV compared to a standard Ag/AgCl reference electrode in 1 M KCl solution (CHI). The potential values reported in this work are referenced to our pseudo Ag/AgCl reference electrode.

3.3. Cyclic voltammetry technique

At the first usage in the electrochemical cell, the ultra-thin ITO film was further stabilized by performing a few scans of cyclic voltammetry (CV) from −0.4 V to +0.8 V with various scan speed (0.02 V/s, 0.1 V/s and 0.2 V/s) until the current signal became stable.

A tungsten–halogen lamp was employed as a broadband light source. The TE polarization was selected by placing a sheet polarizer in the optical path of the incoming beam before arriving at the grating coupler. Additional details of the optical coupling configuration can be found in elsewhere [31]. The out-coupled optical signal was collected by an optical fiber and delivered to a spectrometer that was connected to an intensified CCD (ICCD, Princeton, PI-MAX 3). The out-coupled optical signal under CV potential modulation from −0.4 V to +0.8 V at a

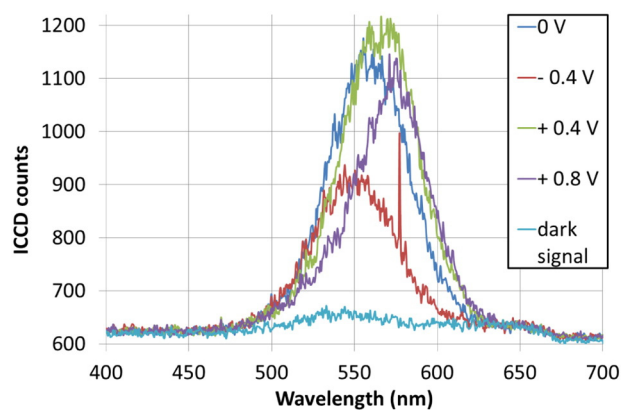


Fig. 3. Power spectrum of the broadband out-coupled guided light at different values of the applied potential during a particular CV scan.

scan-speed of 0.02 V/s was collected. The ICCD was set to an acquisition frequency of 2 Hz with having an exposure time of 200 ms for each frame.

On completion of these measurements, a trace corresponding to a dark signal was collected by injecting black ink into the cell and performing an acquisition under the same exposure time. Fig. 3 shows the out-coupled broadband power spectrum at different values of the electric potential during a particular CV scan.

From the measurements above we calculated the normalized transmittance, t_N , according to Eq. (1) for a particular wavelength:

$$t_N(\lambda) = \frac{I_V - I_{\min}}{I_{\max} - I_{\min}} \quad (1)$$

where I_V is the out-coupled intensity (ICCD counts) at the electric potential V , and I_{\min} and I_{\max} are respectively the minimum and maximum out-coupled intensities at a particular wavelength when the potential was scanned from +0.8 V to −0.4 V over a few cycles. The traces of t_N for a set of discrete wavelengths from 510 nm to 600 nm are shown in Fig. 4. Each wavelength is vertically-shifted by one unit for clarity, and the several cycles of the CV scans are folded into one segment. For a particular wavelength, we observe that the folded traces demonstrate very good repeatability and consistency for the results during the CV

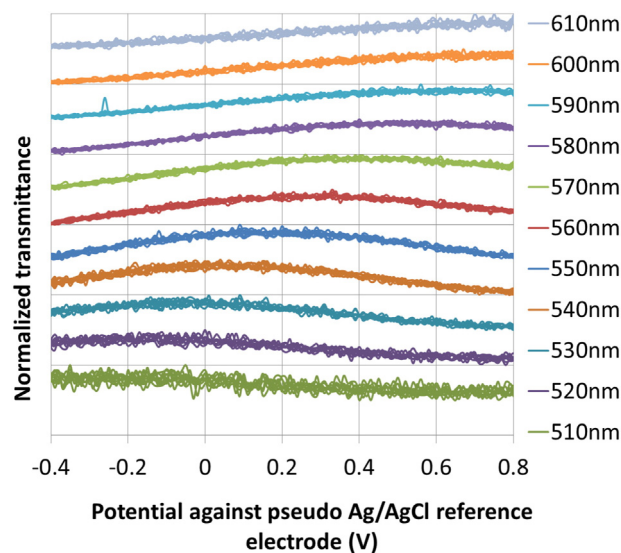


Fig. 4. Normalized transmittance for 3-folded cycles of CV scan obtained from broadband spectrum of Fig. 3. Traces of the transmittance show a clear dependence on the applied potential, and that dependence changes for different wavelengths. For clarity, each curve is shifted by one division.

scans. We also observe that different wavelengths have clearly distinct response to the same potential modulation scan. For example, at 600 nm, the potential of lowest transparency is approximately at -0.4 V, but at 510 nm the potential of lowest transparency is at $+0.8$ V. And for 550 nm, the transmittance shows a peak at about $+0.2$ V.

In the measurements above a light source with a wide spectrum and a broadband waveguide coupler [31] were employed, and the coupling configuration was fixed at a particular geometry to give a band of about 100 nm centered at 560 nm (see Fig. 3). Next, the same protocol of CV potential scans was sequentially applied to several monochromatic laser lines. However, for these following measurements, the flow cell was mounted on a rotation stage so that the incident angle could be adjusted to maximize the coupled light inside the waveguide for each laser line at open circuit potential. The normalized out-coupled transmittance against time (while the applied potential was scanned) is plotted in Fig. 5, as well as the trace for the CV potential scan.

For wavelengths longer than 600 nm, the transmittance follows the potential scan, i.e. they increase and decrease together. At 502 nm, the transmittance and the potential scan change in opposite directions. The normalized transmittance curve at 543 nm shows both behaviors depending on the value of the potential. The folded 5-cycle of normalized transmittance against potential for each laser beam is shown in Fig. 6.

Our measured data show very good consistent between the results obtained with broadband light at a fixed angle (Figs. 3 and 4) and laser lines at their angle of maximum guided light (Figs. 5 and 6). The consistency of these results above shows a clear dependence of the out-coupled optical light intensity on the applied electric potential and suggests two possible lines of explanation. One can hypothesize that the applied potential can either *i*) change the effective refractive index of the IOW device leading to a change in the coupling efficiency or *ii*) change the extinction coefficient of the ITO film leading to a change in the propagation losses. The elucidation of this conundrum is addressed in the next Section, where the first hypothesis was experimentally investigated with measurements of the out-coupled optical intensity against the incident angle for a series of laser lines and at several fixed values of the electric potential to determine if changes in the effective refractive index (due to changes in the applied potential) play an important role in the observed results.

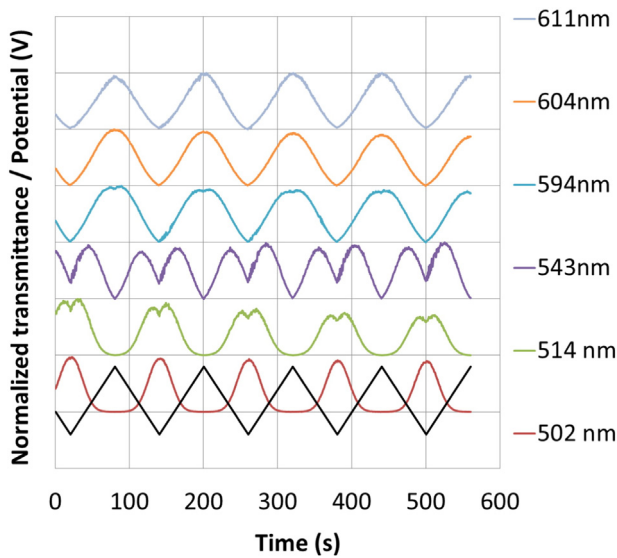


Fig. 5. Normalized transmittance against time for several laser lines under CV potential scan. For clarity each transmission curve is shifted by one division. The trace of the potential modulation is also displayed as the black curve, with the potential ranging from -0.4 V to $+0.8$ V.

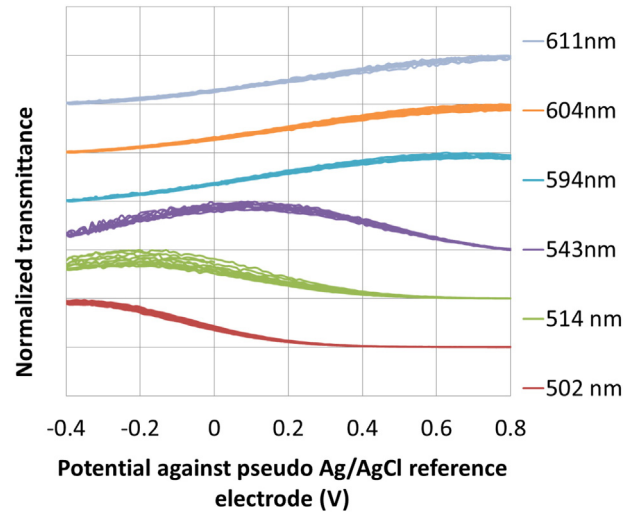


Fig. 6. Normalized transmittance over 5-folded cycles of the applied potential is plotted for each laser line. The results with the laser lines are consistent with the data obtained with the broadband light source (Figs. 3 and 4) and show again the high repeatability of the spectroscopic features during the potential scans. For clarity, each curve is shifted by one division.

3.4. Potential steps technique

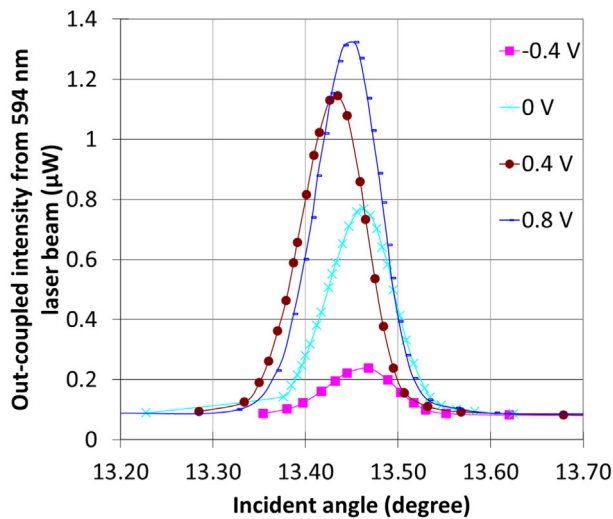
Measurements were taken for several laser lines (502, 514, 543, 594, and 633 nm) at the open circuit condition and for electric potential values of -0.4 , -0.2 , 0.0 , $+0.2$, $+0.4$, $+0.6$, and $+0.8$ V. A polarizer was placed in front of the laser to select the TE polarization, and an achromatic doublet (Thorlabs AC 254-400-A1) with a long effective focal length was employed to collimate the laser beam. The flow cell was mounted on a rotation stage, which allowed us to precisely control the incident angle as we monitor the out-coupled optical intensity at a particular applied potential. For each laser line, we first acquired intensity measurements against the incident angle for the open circuit condition, and then sequentially repeated those measurements at each specific electric potential step listed above. Data for the out-coupled intensity against the incident angle for the 514 and 594 nm laser lines are shown in Fig. 7(a) and (b). We observe in those plots that, for a particular wavelength, the incident coupling angle for the maximum intensity is almost independent of the applied potential. However, at a particular angle of incidence, the intensity shows drastic changes with the applied potential steps. For the 594 nm laser line, the maximum out-coupled intensity at $+0.8$ V potential is more than 6 times larger than the maximum out-coupled intensity at -0.4 V potential, although the coupling angle is about the same (13.45°). For 514 nm laser line, the maximum out-coupled intensity at -0.4 V potential is almost 5 times higher than the maximum out-coupled intensity at $+0.8$ V potential.

By using the incident angle that maximizes the coupled power for each applied potential, the effective refractive index N_{eff} can be calculated as described in Eq. (2), where n_{in} is the refractive index of the incident media (air, in this case), θ_{in} is the coupling angle, λ is the wavelength of the laser line, and Λ is the pitch size of the grating (323 nm).

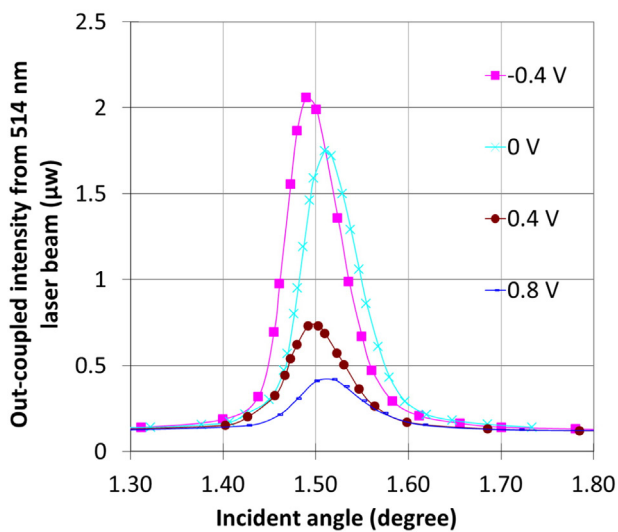
$$N_{eff} = n_{in} \sin\theta_{in} + \frac{\lambda}{\Lambda} \quad (2)$$

The results are shown in Fig. 8, where the effective refractive index calculated for all the laser beams are plotted against the applied potential. It is clear that N_{eff} of the IOW device remains constant when different potential steps are applied to the ultra-thin ITO film.

In addition to the experimental results described above, we note that the thickness of the ITO film used on the IOW device is only 13 nm, and even if the applied potential induces changes in the real part of the



(a)



(b)

Fig. 7. Out-coupled intensity against the input angle for two wavelengths: (a) 594 nm and (b) 514 nm. Measurements were performed at several potential values applied to the ITO film. Not all experimental results (at potential steps -0.2 V, 0.2 V, 0.6 V and open circuit condition) are shown here for the clarity.

refractive index of the ITO film, those effects would have negligible effect on the effective refractive index of the whole IOW device and the coupling conditions would remain unchanged during potential modulations.

These results strongly suggest that the dominant effect for changes in the out-coupled optical power under potential modulations is originated in changes of the extinction coefficient of the ITO (imaginary part of the refractive index). Those changes impact the propagation loss (transmission) and consequently the out-coupled power.

The consistency of this conclusion is further corroborated by comparing the results of the two previous experiments. The normalized transmittance was calculated for the data shown in Fig. 7 (for the 514 and 594 nm) and compared to the equivalent quantity obtained under CV potential scans shown in Fig. 6. For those calculations, displayed in Fig. 9, we used the angle providing the highest out-coupled intensity at the open circuit potential for each potential step because when the data for CV potential scan was collected with the fixed incident angle, the light coupling condition was optimized at the open circuit potential.

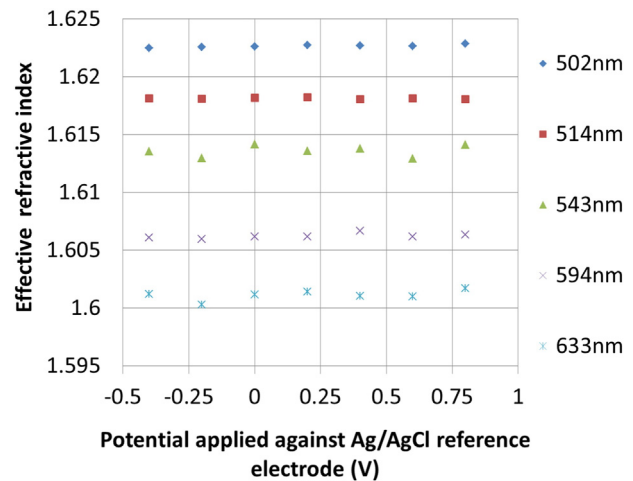
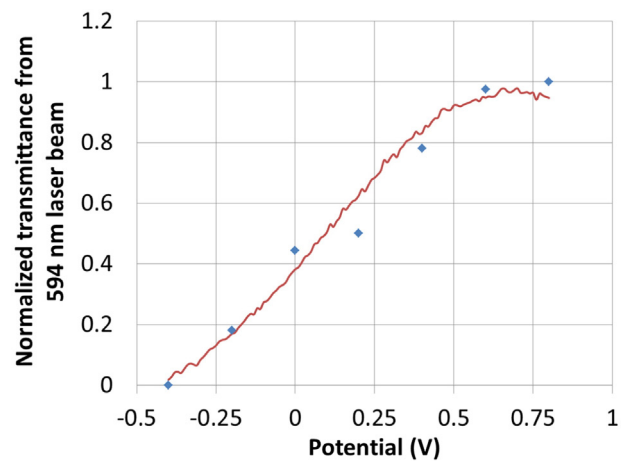
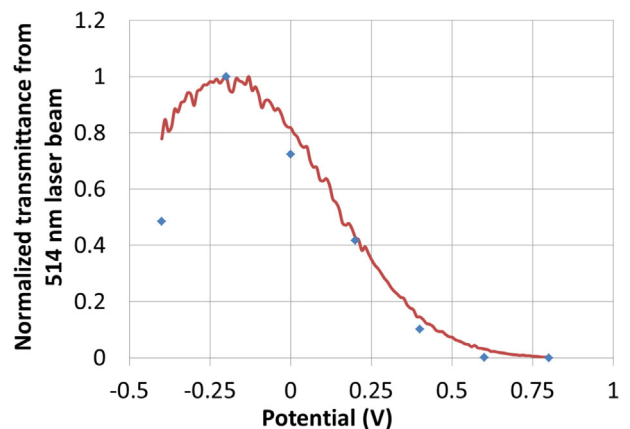


Fig. 8. Effective refractive index for each laser beams at each applied potential step.

The comparisons of the normalized transmittance from these two potential modulation techniques for both the 594 nm and 514 nm are shown in Fig. 9, where we can observe a good agreement for the independent approaches. Similar comparisons from the other laser lines



(a)



(b)

Fig. 9. Normalized transmittance comparison between CV potential scan and potential steps from 594 nm laser line (a) and 514 nm laser line (b). Red solid lines are from CV potential scans, and blue diamonds are from discrete applied potentials.

(data not shown here) also provided good consistent for the measured data obtained by these two types of potential modulations.

3.5. Alternating current potential modulation

Optical measurements with an alternating current (AC) potential modulation applied to the ultra-thin ITO film were also investigated to examine the optical behavior of such structure at different modulation frequencies. For the probing light source, a super continuum fiber laser source (Fianium, SC-400-4) was used. An acousto-optical filter was connected to the fiber laser source to select a specific wavelength with a bandwidth of about 3 nm. The out-coupled intensity of the guided light was collected by a PMT (Hamamatsu R928) and amplified by a current preamplifier (Stanford Research Systems, SR 570). The AC modulated applied potential and optical signals were then collected simultaneously by an oscilloscope (Agilent, DSO8104A Infiniium). A set of AC impedance potential modulations were applied, where each modulation had a fixed DC bias potential (-0.2 V to $+0.28$ V), a constant AC amplitude (10 mV), and a sequence of oscillation frequencies (1 Hz to 20 Hz).

The expression of the AC impedance potential modulation is shown in Eq. (3), where E_{dc} is the potential DC bias, ΔE_{ac} is the AC amplitude, and ω is the angular frequency of the potential oscillation. Under the condition that the AC amplitude is small enough, the optical response can be expressed with a linear approximation, as in Eq. (4), where I_{dc} is the DC term, $\Delta I_{ac,Re}$ and $\Delta I_{ac,Im}$ are the real and imaginary components (respectively) of the modulated optical AC term which include phase delay component.

$$E(t) = E_{dc} + \Delta E_{ac} \sin(\omega t) \quad (3)$$

$$I(t, \lambda) = I_{dc} + \Delta I_{ac,Re} \sin(\omega t) + \Delta I_{ac,Im} \cos(\omega t) \quad (4)$$

The AC components of the optical response in the complex plane (where the real and imaginary components are plotted) are shown in Fig. 10 for (a) 550 nm and (b) 580 nm. The potential oscillation frequency has a clockwise direction from 1 Hz to 20 Hz, as indicated by the black arrows. For the case of the 550-nm probing wavelength, the trace (which is mainly in fourth quadrant) shrinks (ΔI_{ac} decreases) as the potential DC bias increases from -0.2 V to $+0.1$ V and then expands again (mainly in the second quadrant). For the 580 nm wavelength, the optical response is confined to the fourth quadrant under the same interrogation conditions. Those results highlight that both the modulation frequency and the DC bias have an important impact on the optical response of the ITO film. And again, those behaviors are highly dependent on the wavelength under consideration.

The potential DC bias can be interpreted as a constant potential step or the potential point at the slow CV scans. The DC components of the optical signals were compared to the optical response under CV potential scan. The normalized transmittance curves are shown in Fig. 11 for (a) 550 nm and (b) 580 nm separately. For the CV scan, the normalized transmittance was calculated in the potential range from -0.2 V to $+0.28$ V. Good consistent are observed for both probing wavelengths.

4. Discussions

Our data shows that when an ultra-thin ITO film undergoes an electric potential modulation, the out-coupled intensity of a propagating light beam inside the waveguide (which incorporates the ITO film) changes and different probing wavelengths have different profiles. From the experiments under CV scans, potential steps, and AC potential modulations, we were able to conclude that the extinction coefficient (absorption) of the ultra-thin ITO plays a dominant role and has a discernible dependence on the applied potential, and this dependence varies for different wavelengths in the spectral region of the measured data.

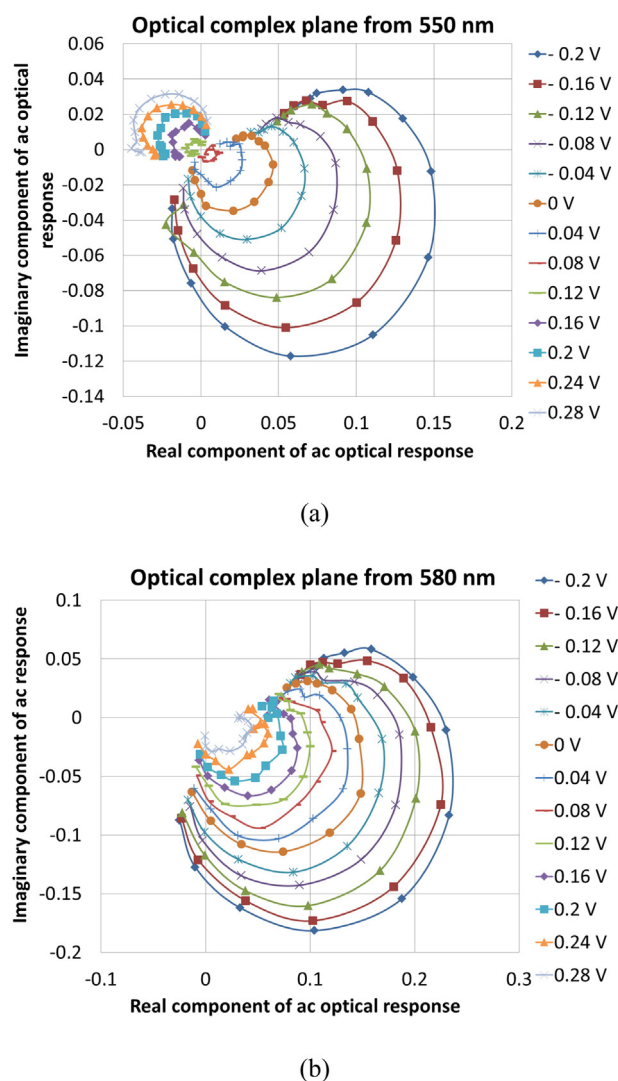
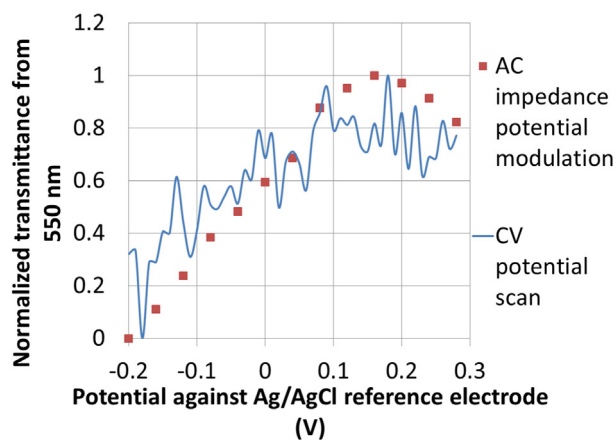


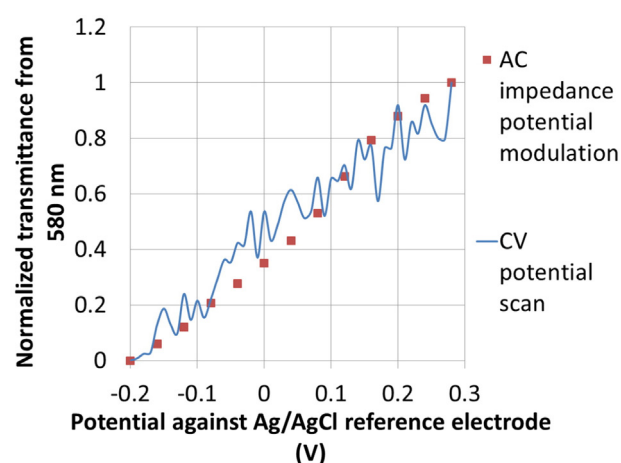
Fig. 10. Complex plane representation of the optical response for an AC-modulation of the applied potential to the ultra-thin ITO film at several potential DC biases for the (a) 550 nm and (b) 580 nm wavelengths. Modulation frequency increases clockwise from 1 Hz to 20 Hz.

As a semiconductor material, the energy band structures of the ITO material have been extensively studied [7]. The optical properties are known to be related to the energy band structures, which are determined by the ratios of the chemical elements indium, tin, and oxygen that form the film. And especially in the visible region, the band structure is dependent on the doping of the tin atom. This phenomenon suggests that the extinction coefficient of ITO film is strongly related to the oxygen vacancy concentration. When a potential modulation is applied to an ultra-thin ITO film, oxygen vacancy concentration could be modified and those vacancies could be changed by Sn element or H⁺ ion diffusion into the film.

The relatively thick ITO films (400 nm) were also tested with acid solution under the similar CV potential scans. With low pH values 4.5 of the electrolyte solution, ITO samples with low O₂ gas flow rate during deposition (0.55 sccm and 0.6 sccm) were darkened in the area immersed in the solution, as shown in Fig. 12. However, ITO samples with higher oxygen content (0.7 sccm O₂ flow rate) were not darkened. This observation further emphasizes the role of the oxygen concentration in the optical properties of the ITO film. Work has been reported with extremely high electrical field on the thick ITO films. With the negative potential, the film was darkened with lower oxygen content, while at positive potential the film resulted in higher oxygen concentration [32].



(a)



(b)

Fig. 11. Comparison of normalized transmittance between the optical DC components from the AC impedance potential modulation and the CV potential scan used a tungsten-halogen white light source. A good agreement is observed for each probing wavelength (a) 550 nm and (b) 580 nm.

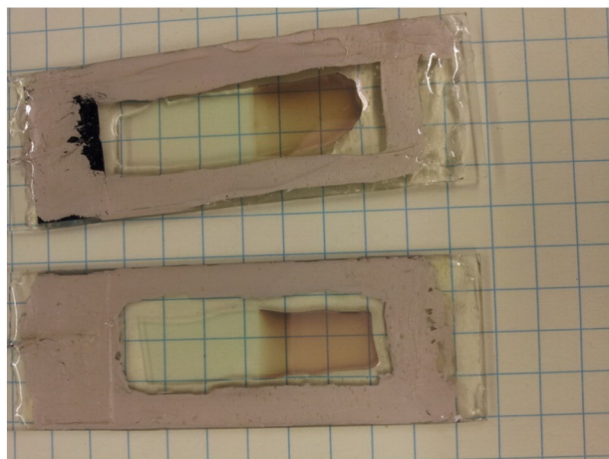


Fig. 12. Picture of a 400 nm thick ITO films under a CV potential modulation in 4.5 pH acid solution.

The spectroscopic properties of the relatively thick ITO films (400 nm) were also tested in the same buffer solution and identical CV potential scans using a UV–Visible spectrophotometer with single transmission technique. No significant change in the transmitted intensity could be detected for these thick films. The reason could be that transmittance measurement is not sensitive enough to show the change from the films since the optical probing length was limited to the thickness of the ITO films or the potential modulation applied on these thick ITO films do not have the same effect as in the ultra-thin ITO films.

5. Conclusions

By exploiting the high sensitivity provided by a single-mode integrated optical waveguide platform, the spectroscopic properties of an ultra-thin (about 13 nm) ITO film deposited on this photonic device were investigated under different potential modulation schemes in the visible spectral region. We confirm through those independent experimental approaches that such thin ITO film exhibits unique spectroscopic features under potential modulations. And those features can be highly relevant and must be taken into consideration in many applications. For example, one area with important applications of the ultra-thin transparent and conductive ITO electrode is for the spectroelectrochemical studies of redox reactions of surface-confined species. The ultra-thin ITO film incorporated into the single-mode integrated optical waveguide has already been demonstrated in redox reaction investigations of a protein layer of cytochrome-c molecules [23]. When a proper analysis of the ITO features discussed here were taken into consideration, experimental data taken under AC potential modulation allowed us to optically retrieve accurate information for the electron transfer rate of this protein assembly adsorbed onto the ITO electro-active interface. And because of the high sensitivity of the single-mode integrated optical waveguide and the high quality of the ultra-thin ITO film, as low as 10^{-14} mol/cm² surface coverage of cytochrome-c proteins were detected under a small (15 mV) amplitude of an AC modulation of the applied electric potential. A multitude of applications based on this electro-active single-mode integrated optical waveguide technology is envisioned for implementation of advanced chemical- and bio-sensing devices and electro-optical characterization of novel solar cells materials.

Acknowledgments

The authors acknowledge financial support from the National Institute of Health (NIH award RR022864), National Science Foundation (NSF EPSCoR award 0814194), and Kentucky Science and Engineering Foundation (KSEF award 1869-RDE-012).

References

- [1] J. Pláa, M. Tamasia, R. Rizzolib, M. Losurdoc, E. Centurionib, C. Summonteb, F. Rubinellid, Optimization of ITO layers for applications in a-Si/c-Si heterojunction solar cells, *Thin Solid Films* 425 (2003) 185–192.
- [2] Supachai Ngamsinlapasathiana, Thammanoon Sreethawongb, Yoshikazu Suzukia, Susumu Yoshikawaa, Doubled layered ITO/SnO₂ conducting glass for substrate of dye-sensitized solar cells, *Sol. Energy Mater. Sol. Cells* 90 (2006) 2129–2140.
- [3] Jin-A Jeong, Han-Ki Kim, Low resistance and highly transparent ITO–Ag–ITO multilayer electrode using surface plasmon resonance of Ag layer for bulk-heterojunction organic solar cells, *Sol. Energy Mater. Sol. Cells* 93 (2009) 1801–1809.
- [4] M. Fahland, P. K., C. Charton, Low resistivity transparent electrodes for displays on polymer substrates, *Thin Solid Films* 392 (2001) 334–337.
- [5] U. Betz, M. Kharrazi Olsson, J. Marthy, M.F. Escolá, F. Atamny, Thin films engineering of indium tin oxide: large area flat panel displays application, *Surf. Coat. Technol.* 200 (2006) 5751–5759.
- [6] C.G. Granqvist, Transparent conductive electrodes for electrochromic devices a review, *Appl. Phys. A* 57 (1993) 19–24.
- [7] C.G. Granqvist, A. Hultaker, Transparent and conducting ITO films new developments and applications, *Thin Solid Films* 411 (2002) 1–5.
- [8] Yung-Chi Yao, Meng-Tsan Tsai, Hsu-Cheng Hsu, Li-Wei She, Chun-Mao Cheng, Chien-Jang Wu, Yi-Ching Chen, Ya-Ju Lee, Use of two-dimensional nanorod arrays with slanted ITO film to enhance optical absorption for photovoltaic applications, *Opt. Express* 20 (2012) 3479–3489.

- [9] Kumar Arunandan, R. Srivastava, M.N. Kamalasanan, Dalip Singh Mehta, Enhancement of light extraction efficiency of organic light emitting diodes using nanostructured indium tin oxide, *Opt. Lett.* 37 (2012) 575–577.
- [10] J.S. Kim, M. Granström, R.H. Friend, N. Johansson, W.R. Salaneck, R. Daik, W.J. Feast, F. Cacialli, Indium–tin oxide treatments for single- and double-layer polymeric light-emitting diodes: the relation between the anode physical, chemical, and morphological properties and the device performance, *J. Appl. Phys.* 84 (1998) 6859–6870.
- [11] Anand Jaina, Giulio Gazzola, Aurora Panzerab, Michele Zanonc, Enrico Marsili, Visible spectroelectrochemical characterization of *Geobacter sulfurreducens* biofilms on optically transparent indium tin oxide electrode, *Electrochim. Acta* 56 (2011) 10776–10785.
- [12] C. Ge, W.J. Doherty 3rd, S.B. Mendes, N.R. Armstrong, S.S. Saavedra, Voltammetric and waveguide spectroelectrochemical characterization of ultrathin poly(aniline)/poly(acrylic acid) films self-assembled on indium–tin oxide, *Talanta* 65 (2005) 1126–1131.
- [13] Chih-Hao Lianga, Sheng-Chau Chena, Xiaoding Qib, Chi-San Chena, Chih-Chao Yang, Influence of film thickness on the texture, morphology and electro-optical properties of indium tin oxide films, *Thin Solid Films* 519 (2010) 345–350.
- [14] F. Wang, M.Z. Wu, Y.Y. Wang, Y.M. Yu, X.M. Wu, L.J. Zhuge, Influence of thickness and annealing temperature on the electrical, optical and structural properties of AZO thin films, *Vacuum* 89 (2013) 127–131.
- [15] T.C. Gorjanca, D. Leong, C. Py, D. Roth, Room temperature deposition of ITO using r.f. magnetron sputtering, *Thin Solid Films* 413 (2002) 181–185.
- [16] Dong-Ho Kim, Mi-Rang Park, Hak-Jun Lee, Gun-Hwan Lee, Thickness dependence of electrical properties of ITO film deposited on a plastic substrate by RF magnetron sputtering, *Appl. Surf. Sci.* 253 (2006) 409–411.
- [17] A.L. Swint, P.W. Bohn, Effect of the interfacial chemical environment on in-plane electronic conduction of indium tin oxide role of surface charge dipole magnitude, and carrier injection, *Langmuir* 20 (2004) 4076–4084.
- [18] E. Matveeva, Electrochemistry of the indium–tin oxide electrode in 1 M NaOH electrolyte, *J. Electrochem. Soc.* 152 (2005) H138–H145.
- [19] Dai Kato, G. Xue, Yuzuru Iwasaki, Yoshiki Hirata, Ryoji Kurita, Osamu Niwa, Heavy phosphate adsorption on amorphous ITO film electrodes nano-barrier effect for highly selective exclusion of anionic species, *Langmuir* 23 (2007) 8400–8405.
- [20] F. Nüesch, E.W. Forsythe, Q.T. Le, Y. Gao, L.J. Rothberg, Importance of indium tin oxide surface acidity for charge injection into organic materials based light emitting diodes, *J. Appl. Phys.* 87 (2000) 7973–7980.
- [21] Er-Jia Guo, Haizhong Guo, Huibin Lu, Kuijuan Jin, Meng He, Guozhen Yang, Structure and characteristics of ultrathin indium tin oxide films, *Appl. Phys. Lett.* 98 (2011) 011905–3.
- [22] S. Stankowski, J.J. Ramsden, Voltage-dependent coupling of light into ITO-covered waveguides, *J. Phys. D: Appl. Phys.* 35 (2002) 299–304.
- [23] L.R. Cruza, C. Legnania, I.G. Matosoa, C.L. Ferreira, H.R. Moutinho, Influence of pressure and annealing on the microstructural and electro-optical properties of RF magnetron sputtered ITO thin films, *Mater. Res. Bull.* 39 (2004) 993–1003.
- [24] R. Swanepoel, Determination of the thickness and optical constants of amorphous silicon, *J. Phys. E Sci. Instrum.* 16 (1983) 1214–1222.
- [25] D.R. Dunphy, S.B. Mendes, S.S. Saavedra, Neal R. Armstrong, The Electroactive integrated optical waveguide ultrasensitive spectroelectrochemistry of submonolayer adsorbates, *Anal. Chem.* 69 (1997) 3086–3094.
- [26] D. Mergel, Z. Qiao, Correlation of lattice distortion with optical and electrical properties of In₂O₃:Sn films, *J. Appl. Phys.* 95 (2004) 5608–5615.
- [27] John Thomas Bradshaw, S.B. Mendes, Neal R. Armstrong, S. Scott Saavedra, Broadband coupling into a single-mode, electroactive integrated optical waveguide for spectroelectrochemical analysis of surface-confined redox couples, *Anal. Chem.* 75 (2003) 1080–1088.
- [28] R.S. Wiederkehr, G.C. Hoops, M.M. Aslan, C.L. Byard, S.B. Mendes, Investigations on the Q and CT bands of cytochrome c submonolayer adsorbed on an alumina surface using broadband spectroscopy with single-mode integrated optical waveguides, *J. Phys. Chem. C* 113 (2009) 8306–8312.
- [29] Rodrigo S. Wiederkehr, H.C. Geoffrey, Sergio B. Mendes, Effects of sodium chloride on the properties of chlorophyll a submonolayer adsorbed onto hydrophobic and hydrophilic surfaces using broadband spectroscopy with single-mode integrated optical waveguides, *Opt. Eng.* 50 (2011) 071109–8.
- [30] M.B. Pereira, J.S. Craven, S.B. Mendes, Solid immersion lens at the aplanatic condition for enhancing the spectral bandwidth of a waveguide grating coupler, *Opt. Eng.* 49 (2010) 124601–124608.
- [31] J. He, M. Lu, X. Zhou, J.R. Cao, K.L. Wang, L.S. Liao, Z.B. Deng, X.M. Ding, X.Y. Hou, S.T. Lee, Damage study of ITO under high electric field, *Thin Solid Films* 363 (2000) 240–243.
- [32] X. Han, S.B. Mendes, Optical impedance spectroscopy with single-mode electroactive-integrated optical waveguides, *Anal. Chem.* 86 (2014) 1468–1477.